crystals

MDPI

Article

Highly Efficient and Multiband Metamaterial Microstrip-Based Radiating Structure Design Showing High Gain Performance for Wireless Communication Devices

Ammar Armghan [1,*], Sunil Lavadiya [2], Meshari Alsharari [1,*], Khaled Aliqab [1], Malek G. Daher [3] and Shobhit K. Patel [4]

[1] Department of Electrical Engineering, College of Engineering, Jouf University, Sakaka 72388, Saudi Arabia
[2] Department of Information and Communication Technology, Marwadi University, Rajkot 360003, India
[3] Physics Department, Islamic University of Gaza, Gaza P.O. Box 108, Palestine
[4] Department of Computer Engineering, Marwadi University, Rajkot 360003, India
* Correspondence: mmaalsharari@ju.edu.sa (M.A.); aarmghan@ju.edu.sa (A.A.)

Abstract: High-speed wireless communication devices need antennas to operate at multiple frequencies with high gain. The need for such antennas is increasing day by day. The proposed metamaterial superstrate antenna gives a high gain and multiband performance, which is required in high-speed wireless communication devices. The designed antenna is also applicable for C- and X-band communication devices. The structure consists of a simple patch and multiple split-ring resonator metamaterials on the superstrate region. The performance optimization is achieved by adjusting the feed position, varying the height of the superstrate layer and changing the thickness of metamaterial rings. The proposed design is analyzed for 4 GHz to 12 GHz. The performance analysis regarding the reflection coefficient, directivity, gain and electric field is observed. FR4 is used as a dielectric material that makes the design low-cost. The proposed design represents a minimum reflection coefficient response of −49 dB, a bandwidth of 490 MHz, a maximum electric field of 1.29×10^4 v/m, good directivity and a broader radiation pattern. The comparison between the simulated and the measured results is incorporated in the manuscript. A comparison of the presented design with other articles is included to check the novelty of the design. The proposed method helps to target applications such as WiFi, Earth observation and microwave links.

Keywords: metamaterial; high gain; multiband; bandwidth; directivity

Citation: Armghan, A.; Lavadiya, S.; Alsharari, M.; Aliqab, K.; Daher, M.G.; Patel, S.K. Highly Efficient and Multiband Metamaterial Microstrip-Based Radiating Structure Design Showing High Gain Performance for Wireless Communication Devices. *Crystals* **2023**, *13*, 674. https://doi.org/10.3390/cryst13040674

Academic Editors: Kerlos Atia Abdalmalak, Raed Shubair, Ayman Althuwayb, Bal S. Virdee and Yuri Kivshar

Received: 16 February 2023
Revised: 6 April 2023
Accepted: 11 April 2023
Published: 14 April 2023

1. Introduction

The use of wireless networks for various purposes is expanding quickly. To accommodate more features in the limited size, antennas must continue to shrink significantly when mobile devices shrink or pack in more functionality. In addition, the need for antennas that can function across several frequency bands has increased as the number of frequency bands in use has increased [1]. To fulfill these space-saving prerequisites, compact and multiband antennas are required. It is common practice to use various resonances and impedance matching techniques to accommodate the integration of tiny antennas in small packaging. As a result, researchers and practitioners alike have a strong interest in antennas that are both small and capable of handling several frequencies. The employment of multiple resonance techniques has been the primary focus of research into these antennas [2]. One of the most significant aspects of an ongoing investigation into the system level is to incorporate wideband and multiple-band response, even though maintaining proper radiation pattern and miniaturizing antenna are the two most present issues [3]. Smartphones, laptops and other personal terminal devices are more commonplace as wireless technology advances. As a result, multiband antennas for WLAN and WiMAX have been designed due to the high demand for these technologies in our portable terminals [4,5].

To achieve multiband performance, many techniques have been devised, such as using different branches in the patch region and each of them resonating at a different frequency [6], Loading and shorting an the inner and outer area of the patch [7], slotting a few areas of the patch [8], the fractal shape of the patch elements, T-shaped fractal antenna for provides the six band response [9], The antenna structure with E and a shaped stub helps to attain the seven band response with less than −10 dB of the reflection coefficient [10], The article [11] represents using the coupled feed mechanism wide band characteristics being achieved with the multiband response, while cutting the patch region using the inverted HE shape provides the four band response [12], The rectangular microstrip patch with a U-shaped slot and two concentric annular slots to help the sleeved meanders are added in the ground plane to alter the surface current distribution, which improves the antenna's bandwidth and multiband response. The artificial neural-based approach uses a fractal antenna to target C and X-band communication applications [13].

The mentioned articles are poor impedance matching, less gain and an improper reflection coefficient response; therefore, the solution is attained using the metamaterial concept. Recently, there has been a significant increase in the number of scientists looking at metamaterials. For example, negative permittivity and negative permeabilities may be created when these components are alternated regularly in metallic structures [14]. With the development of metamaterial technology, designers of multiband antennas now have a new tool. Split-ring resonators are the most common type of primary metamaterial unit cells. It is possible to achieve multiband features by engraving unit cells directly into the substrate and ground plane [15]. In this context, metamaterials' unique electromagnetic characteristics have attracted much interest. To reduce the antenna dimensions, the metamaterial approach may be used. Metamaterial will also help to modify the near-field boundary conditions. Antenna designers face more than only the difficulties of downsizing in their work. Few products, such as communication handsets, feature considerable free space for an antenna. The device also necessitates that the radiating element function over a wide range of operating frequencies to accommodate its wide variety of applications. Adopting a single antenna that can transmit and receive on all of these frequencies might solve this problem while keeping the device's footprint to a minimum. The solution using metamaterial-based approach is presented in following articles. The circular-shaped CSRR-based fractal antenna [16], the fidget-shaped structure loaded with parasitic SRR for multiband wireless communication applications [17], The monopole antenna lotus shaped for X-bands and WLAN is proposed using the metamaterial and partial ground concept, Article [18] provides a dual-polarized slot antenna using SRR at the C-band. Using eight SRRs between two ports as the suggested architecture achieves excellent inter-port isolation and a low axial ratio. A reflector near the feed line has also been used to boost the design's modest gain. The article proposed in [19] represents the C-shaped metamaterial elements in monopole antenna that provide the multiband response, and the design is appropriate for the WiMAX and GSM applications. The WiMAX and WLAN applications are supplied by the Coplanar Waveguide (CPW). A unique substrate-integrated magneto-electric dipole antenna with circular polarization was developed to provide efficient wireless communication. The antenna consists of a ground plane, two rows of metallic vias printed in arc shapes and a feeding strip on top. The antenna can provide consistent and unidirectional radiation over its entire working frequency range. This layout has the potential to work for small and lightweight wireless transceivers operating in the sub-6 GHz band or for use in satellite communications [20]. A hybrid half-mode substrate-integrated waveguide diplex antenna is presented for wearable transceiver purposes. The antenna has a circular and rectangular cavity, both quarter-mode structures. Using separate microstrip lines to stimulate each resonator, it has two independent resonance frequencies of 4 GHz and 4.79 GHz. By etching a rectangular slit at the cavity junction, we may ensure a high degree of isolation (>25 dB) between the two resonator cavities [21].

Ref. [22] represents one rectangular slot with an open end installed on the top cladding of a compact half-mode substrate-integrated waveguide. The slot splits the cavity into two

unequal apertures. Isolation of more than 25 dB may be achieved with careful and adequate optimization of the antenna size, which also helps to initiate the self-duplexing feature. The suggested design uses a low-cost printed circuit board to actualize it on a single-layered dielectric substrate. To increase isolation for 5G millimeter wave applications, a low-profile planar MIMO antenna with four components is suggested in [23]. The microstrip feeds a slanted spade-shaped radiator with four asymmetrical slots and a partial ground plane that serves as one of the MIMO antenna's radiating elements. The isolation between the antenna components is then strengthened by loading two cross lines in that space. The design's analysis was carried out using a parametric examination of the dimensions of the whole and split-ring resonators, the distance between the feeding ground planes, the thickness of the substrate and the various dielectric constants. Broad bandwidth is achieved by this approach [24]. The optimization of the different parameters helps design an optimized antenna, which gives better gain and bandwidth that can be utilized for other applications. The design uses C.SRR to investigate the potential of a multilayer, dual-polarized antenna inspired by metamaterials.

A metasurface ground plane and a slotted square patch filled with CSRR are planned to sit atop two substrates in this architecture. The antenna shows various radiation properties, making it suitable for LTE, WiMAX and satellite use. The article delves into using a square CSRR in a UWB MIMO antenna with a forked configuration. U and Z slot-based antenna and a CSRR combine to produce a two-element multiple-input multiple-output structure in the antenna's unit cell. For use in a variety of applications among the frequency bands 2 GHz and 9 GHz, a circular fractal antenna equipped with a spectral response ring was developed. Using an SRR-loaded antenna has been shown to increase both gain and bandwidth, making it a promising candidate for WiMAX deployments [25].

The suggested design has multiband operating frequencies as well as a high gain. The proposed architecture is intended for fixed satellite services such as radio location identification and different wireless communication services. The antenna's performance has been enhanced by reflection coefficient, gain and bandwidth. The simulated and measured results of the suggested design are in excellent agreement. The presented article is structured as follows: Section 2 analyzes the proposed antenna's design concerns, including dimensions characterization, far-field resonance behavior and parametric research of several associated dimensional factors. Section 3 depicts the performance metrics. Section 4 reflects the design's uniqueness compared to previous works, and the Section 5 summarizes the conclusion.

2. Contribution of Proposed Structure

There is a trade-off between the device size, the number of operating bands, the average gain and the undesirable distortion in the radiation characteristics. Although the antennas reported in the literature have a high gain and are multiband, there is a trade-off among many factors. Incorporating metamaterial and slots into the design of a miniaturized multiband antenna to achieve acceptable gain across all of the operating bands is the overarching goal of the study, which has been presented to solve the design problems that have been outlined above. The following is an outline of the primary contributions, novelty and advantages of this work:

- The proposed simple structure helps to attain the multiband response to cover a broad range of applications.
- A metamaterial slot antenna with a high gain and the ability to operate on six different bands is presented for use in WLAN and earth observation applications.
- To achieve a multiband response, optimization of the feed point and changing the superstate layer's height are carried out.
- The simulation and fabrication were performed using the low-profile FR4 substrate material.
- The antenna consists of a straightforward patch construction and a superstate design influenced by metamaterial rings.

- The addition of metamaterial rings in the patch gives a better response to the superstrate antenna design.
- The varying size of metamaterial rings carries out the optimization of the reflection coefficient.
- The study includes comparing the findings of simulation and measurements and the fabrication of an antenna construction employing low-profile FR4 material.
- The structure provides the minimum reflection coefficient of −49 dB with a bandwidth of 400 MHz.
- To determine the extent of the improvement, a comparison of the work being conducted here with that of other articles is included.

3. Antenna Structure Design

The primary goal of this effort is to achieve a multiband response using the metamaterial principle. Microstrip antennas radiate because of the presence of fringing fields. The presence of fringing fields may explain the radiating action of the microstrip antenna. Patch have the highest current in their midst and the lowest current at their ends. As the patch antenna may be considered an open-circuited transmission line, its voltage reflection coefficient will equal one. If this occurs, the voltage and current are out of phase. Hence, the voltage peaks as the patch nears its end. Around the patch antenna's origin, the voltage has to be at its half-wavelength distance. Therefore, the fields underneath the patch will look like the fringe fields on the patch's edges. Microstrip antenna radiation is the sum of the phase-added E-fields surrounding the antenna. Fringing fields are responsible for the microstrip antenna's emission. The metamaterial approach is used to attain multiband phenomena because they have the advantages of offering wideband, miniaturization and simplicity of integration with different portable devices. Thus, it serves as a viable alternative for constructing multiband antennas. The metamaterial ring loading over the superstrate region will also help to achieve excellent gain as well as provide strengthening of the structure.

The proposed three-dimensional design is shown in Figure 1a. The design comprises a simple patch antenna, and the four SRRs are loaded in the superstrate region. The four SRRs enable metamaterial properties in the design. The view of the represented design is observed in Figure 1b. The lateral view of the proposed design is shown in Figure 1c. The size of the square-shaped radiating patch element is 39.2 mm. The overall size of the substrate is 48.2 mm. The overall outer dimensions of the fourth SRR are 35.3 mm. FR4 material is a dielectric material with 4.4 dielectric constants [26]. The lower cost of FR4 helps with mass production and FR4 provides ease of fabrication. The thickness of the substrate and superstrate region is 1.6 mm. The thickness of the ground, patch and four SRRs is 1.6 mm. The patch region is excited by applying input through the coaxial feed.

The metamaterial ring is loaded in the superstrate region. There are four SRRs loaded in the superstrate area. The overall dimensions of the four SRRs are lower than the patch area. The resonance frequency of the presented design was calculated using Equations (1) and (2). The metamaterial unit cell is positioned above the inset feed's square patch. As a result, the square-shaped metamaterial ring is smaller in size than the square-shaped patch.

$$f_r = \frac{X_{mn}}{2\pi a_{e\sqrt{\varepsilon_r}}} c \tag{1}$$

$$a_e = a\left\{1 - \frac{2\mathrm{h}}{\pi \mathrm{a}\varepsilon_r}\left(\ln\frac{\pi \mathrm{a}}{2\mathrm{h}} + 1.7726\right)\right\}^{1/2} \tag{2}$$

where f_r represents the resonating frequency, ε_r is the relative permittivity, a_e is the effective dimension of the ring, The speed of light is represented by c, and the substrate height is h. Finally, the conventional resonance of the cavity is expressed using Equation (3).

$$H + t\sqrt{\varepsilon_r} = (\varnothing_{MS} + \varnothing_G)\frac{\lambda}{4\pi} \pm N\frac{\lambda}{2} \quad (3)$$

The ground plane reflected phase is $\varnothing_G$, and $\varnothing_{MS}$ is the reflecting phase of the metamaterial element. N is an integer, and the thickness of the metamaterial substrate is t. Changing the value of H creates a resonance cavity where multiple reflections occur between the patch antenna's ground plane and the metamaterial cell superstrate. An enhancement in antenna gain is possible if the antenna satisfies the standard resonance cavity condition because the reflected waves will go through the unit cell at the same phase as the original wave [27]. The presented structure is fabricated and verified to identify the performance index of the proposed work. Figure 2 represents the modeled design with the test setup.

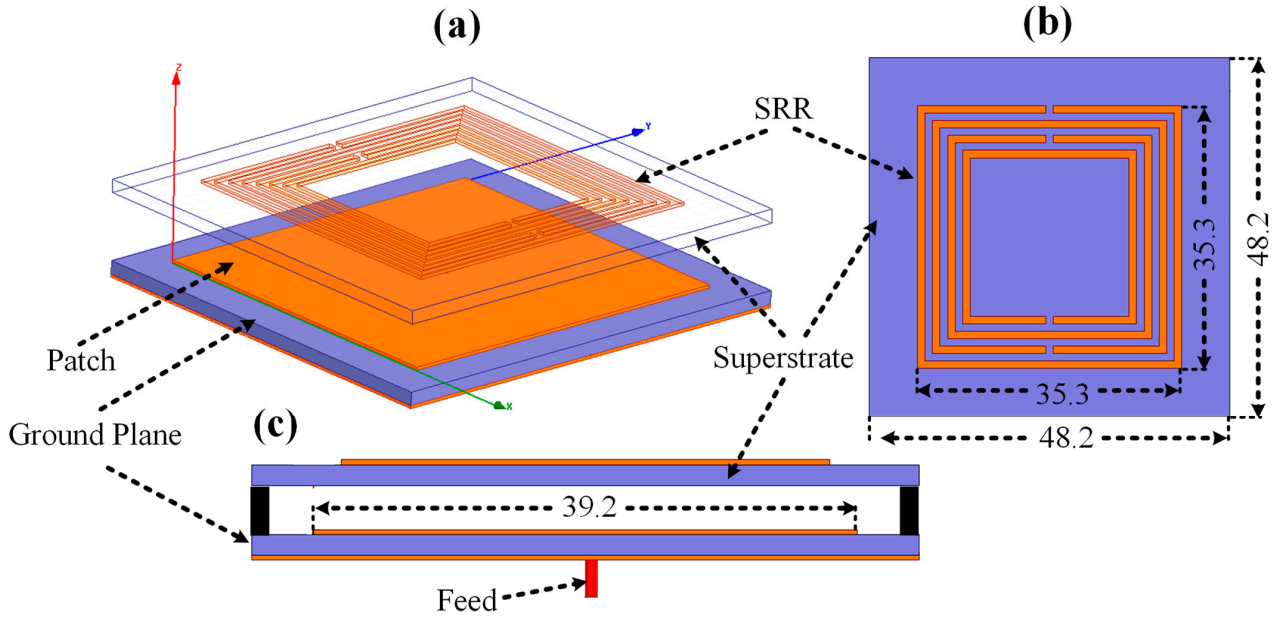

Figure 1. (**a**) 3D view of the presented structure. (**b**) The upper view of the metamaterial ring-loaded structure. (**c**) The side view of the proposed structure.

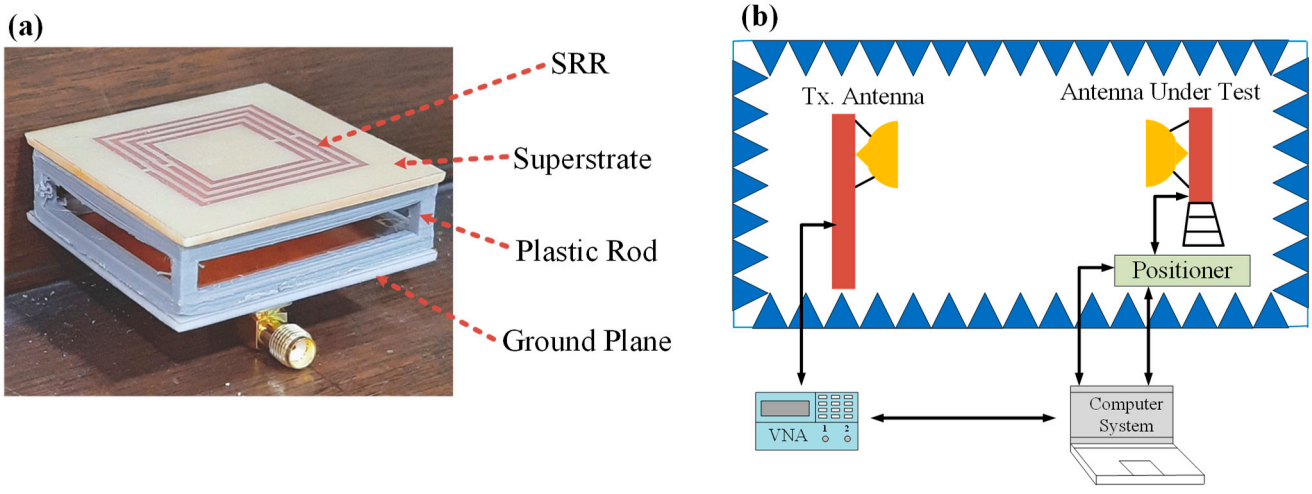

Figure 2. (**a**) Fabricated view of the proposed design structure. (**b**) Antenna test setup for testing.

4. Result and Discussion

The design is analyzed by considering the perfect electric conductor in the ground and patch material. Still, during the fundamental analysis of the prototype, due to the lossy behavior of the material, different performance characteristics such as the reflection coefficient and radiation pattern will provide a slightly different response compared to the ideal situation. The minor shape variation in the prototype-making affects the performance of the structure. The real-time analysis of varying performance indicates design, noise, weather conditions and many other things that will affect the performance [28]. Linearity and time-invariance are often used as assumptions to make issues more manageable. However, there were excellent reasons to grow entrenched in the LTI assumption, and it may now be too constraining for antenna engineers.

Nevertheless, the LTI assumption is very useful in a few crucial areas. One advantage is that it simplifies computations and models, which has traditionally been a required step due to limited processing capability [29]. The performance analysis of the design is carried out using the scattering parameters at high frequency. The input is applied using the coaxial feed. The input from the feed energizes the patch of the structure that generates the fringing field effect, and accordingly, the antenna starts the radiation. The minimum value of the scattering parameter represents better performance. The primary purpose of the proposed design is to target the maximum number of applications using the single antenna; the multiband response helps to achieve multiple applications [30]. Few analyses are carried out to accomplish the multiband response with better performance. The first analysis is to vary the feed position from the outer corner to the center. The variation is moved in diagonally. The outermost part is 1 mm, and the maximum shift point is 20 mm. The Fermi plot response is represented in Figure 3. The Fermi plot indicated the effect of the reflection coefficient response for the diverse value of feed position. The Fermi plot means there are multi-band responses based on color variation. The red color indicates the value near zero, and the color variation from red to blue represents reducing the reflection coefficient response. It is clear from Figure 3 that the multiband response for the feed position at 1 mm. Therefore, the optimization of the reflection coefficient response for the different feed values is identified. Figure 4 represents the line plot for different feed positions. Initially, the distinct value of the feed point values varied from the outer to the inner side. There is multiband resonance observed from the different feed positions. Therefore, based upon the analysis in terms of S_{11} and gain plot, the optimum value considered is 1 mm.

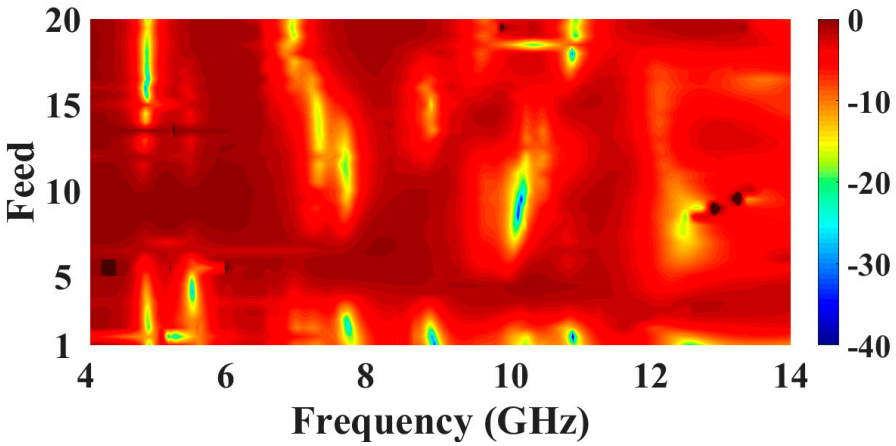

Figure 3. The reflection coefficient response plot over different feed positions 1 mm to 20 mm.

The second analysis is carried out for improving the reflection coefficient by adjusting the height of the superstrate region over the patch element. The superstrate concept helps to achieve multiband response, better gain and bandwidth enhancement. It also allows for enhancing the strength of the material [31]. The effect of superstrate height above the patch area for the reflection coefficient response is represented in Figure 5. The field confinement

of the structure is also enhanced due to the concept of the superstrate. A trade-off must be performed as the gap size among the patch and superstrate region increases and the overall dimensions increase. The superstrate's height varies from 0 mm to 3 mm. The line plot of the gap variation is shown in Figure 6. The height variation makes the reflection coefficient response more confined. The optimized size of 2 mm is achieved to target the multiband response. The bands are a little bit shifted as per the gap variation.

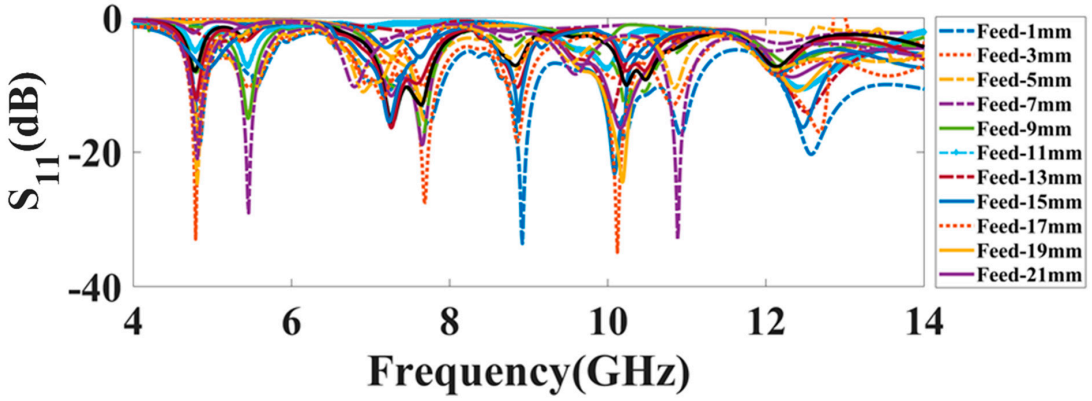

Figure 4. The line plot of S_{11} for different feed positions. The 1 mm is considered an optimum feed position.

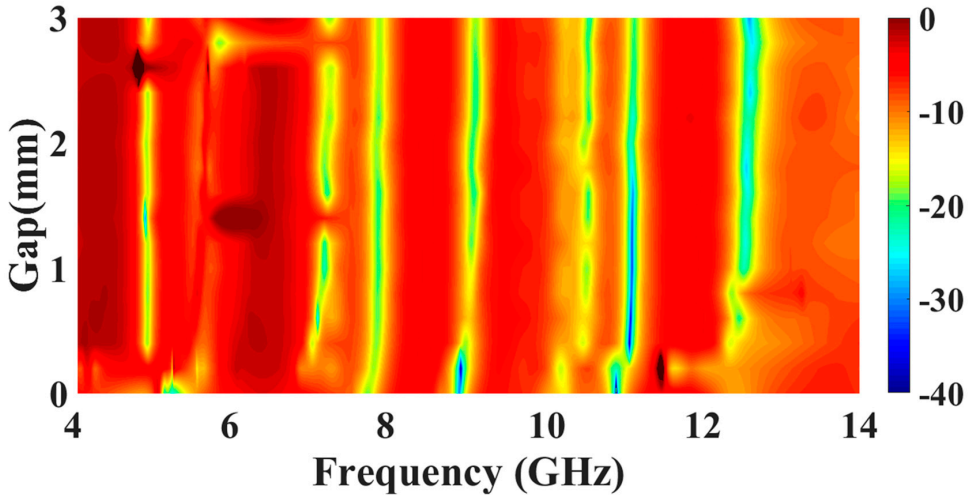

Figure 5. Superstrate height variation over the 0 mm to 3 mm for analysis of reflection coefficient response.

There are four split-ring resonators loaded at the top of the superstrate area. The superstrate approach helps to improve the performance of the structure. The width of SRR change over the 1 mm to 4 mm range is observed in Figure 7. The width variation leads toward minimizing the reflection coefficient response. Overall variation in the dimension of the SRR is not majorly affected by the reflection coefficient response. The optimized reflection coefficient response is achieved for the SRR thickness of 1mm. The size variation of the metamaterial rings will affect the charge distribution concentration, which results in a variation in the structure's performance. The dimensions of the rings should be proper to avoid minimum variation in the simulated and measured response. The fourth analysis in the proposed design is taken by changing the number of rings to check the reflection coefficients. The optimum value of all the parametric studies is considered for the analysis, as shown in Figure 8. The graph shows that the variation of different parameters will affect the reflection coefficients. The shifting of bands with the variation in the reflection coefficients is observed.

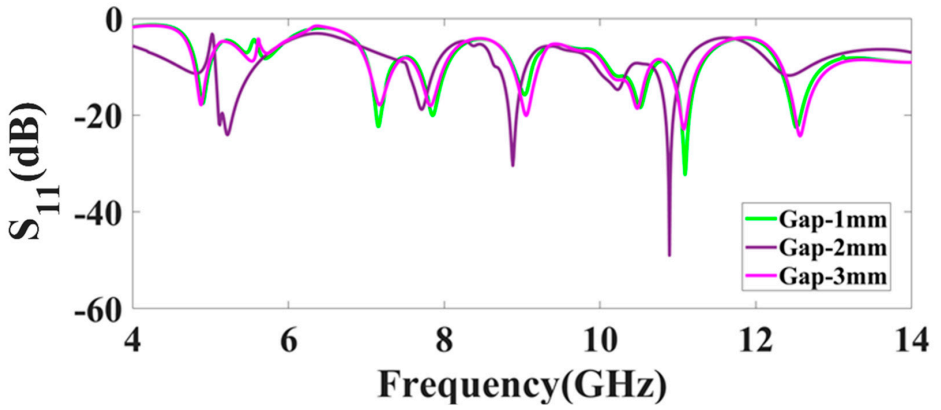

Figure 6. The line plot of S_{11} for different gap positions among patch and superstrate layer. The 2 mm gap is considered optimum.

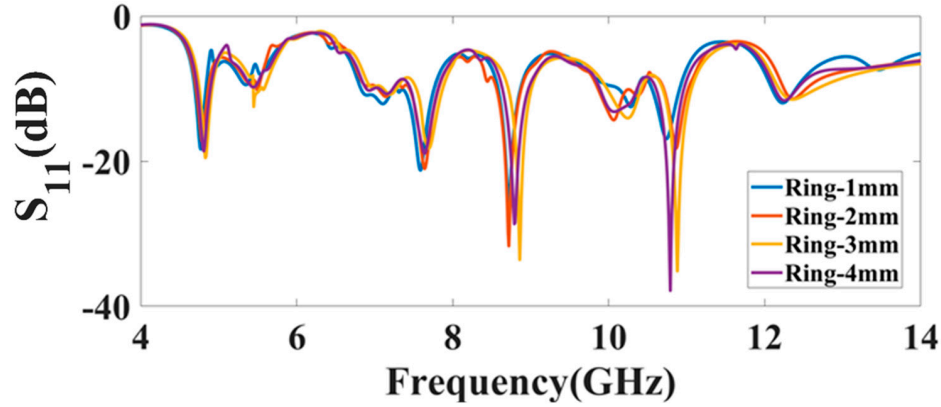

Figure 7. The reflectance (S_{11}) response observation for the multiple values of SRR thickness. The variation was carried out over 1 mm to 4 mm. The optimized multiband response was achieved for the 4 mm of SRR thickness. The response is observed throughout 4 GHz to 14 GHz.

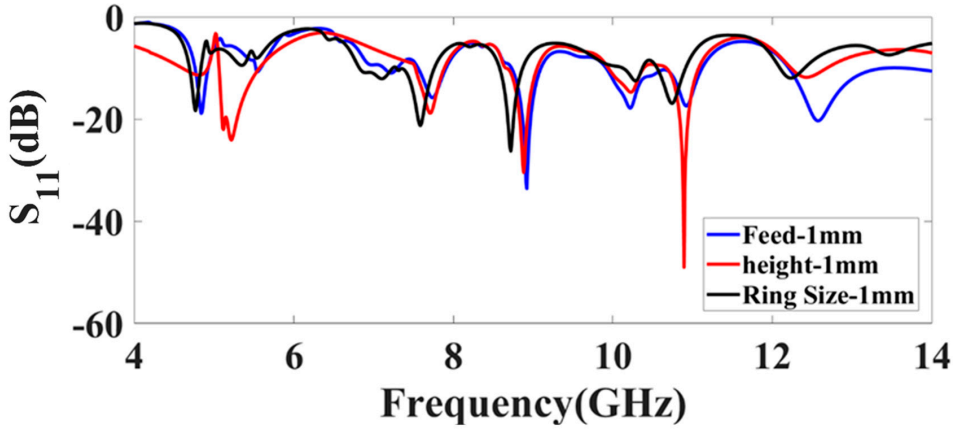

Figure 8. The optimized parametric analysis of variations such as the feed position, gap among patch and superstrate and ring size variation.

Figure 9 represents the parametric study for the effect of the reflection coefficient for the different metamaterial rings. The multiband response is observed for all the configurations. Figure 9a shows the minimum S_{11} of −25.83 dB at 10.804 GHz with a peak bandwidth of 400 MHz over 9.904 GHz to 10.304 GHz. Figure 9b shows the minimum S_{11} of −23.25 dB at 10.8 GHz with a peak bandwidth of 406 MHz over 9.904 GHz to 10.310 GHz. Figure 9c shows the minimum S_{11} of −24.46 dB at 10.79 GHz with a peak bandwidth of 410 MHz over 10.004 GHz to 10.414 GHz. Figure 9d shows the minimum S_{11} of −49 dB at 10.891 GHz with

a peak bandwidth of 400 MHz over 10.671 GHz to 11.071 GHz. Out of all the configurations, the minimum reflection coefficient of −49 dB is achieved in the four-ring designs.

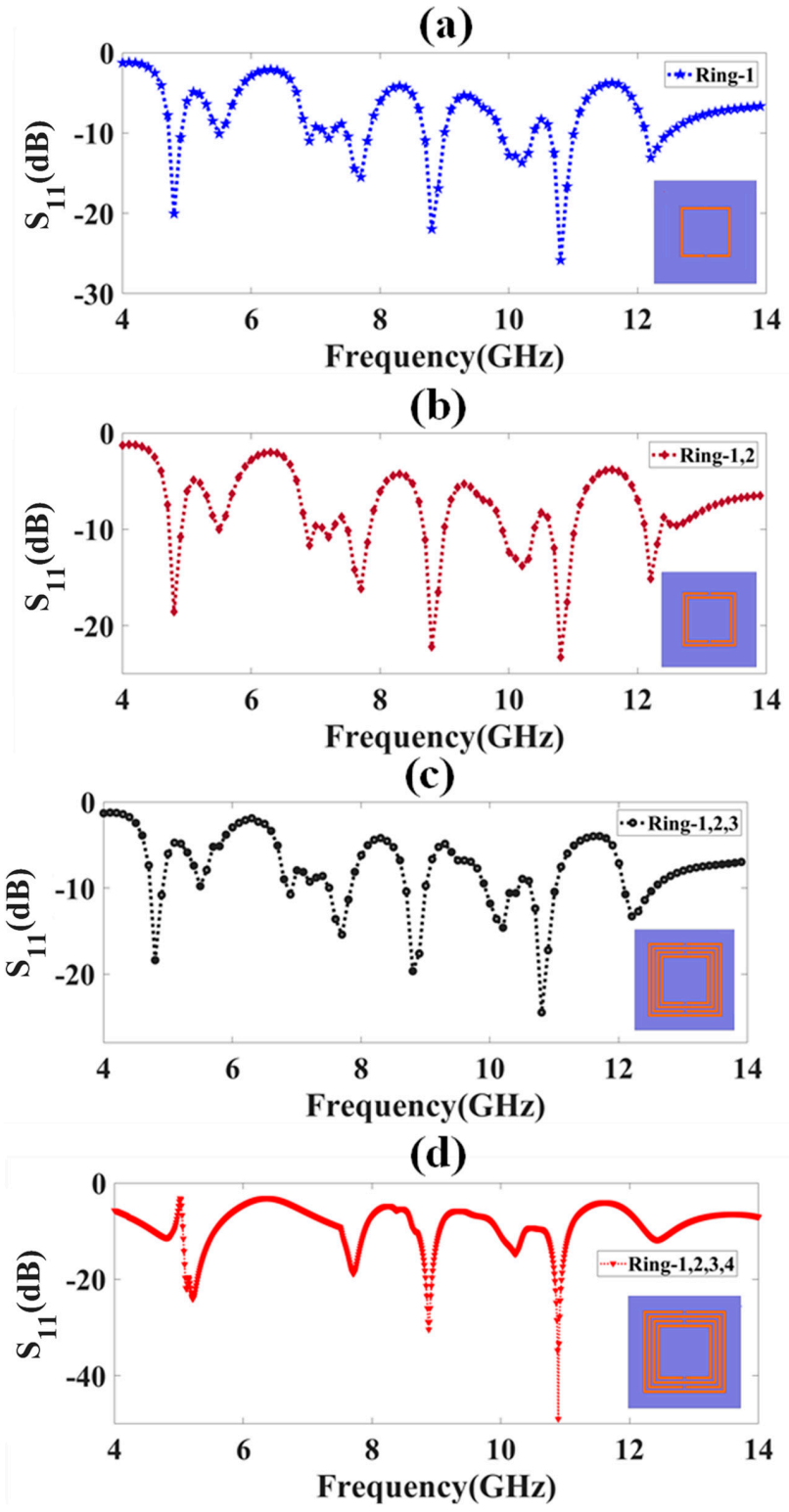

Figure 9. Reflection coefficient analysis for different metamaterial rings. (**a**) Minimum S_{11} of −25.83 dB and peak BW of 400 MHz attained for one ring structure. (**b**) Minimum S_{11} of −23.25 dB and peak BW of 406 MHz achieved for one ring structure. (**c**) Minimum S_{11} of −24.46 dB and peak BW of 410 MHz attained for one ring structure. (**d**) Minimum S_{11} of −49 dB and peak BW of 400 MHz achieved for one ring structure.

The proposed design is numerically simulated and fabricated using the FR4 material. The reflection coefficient of the proposed optimized design is observed in Figure 10. The comparison between the measured and the simulated responses is kept. The similarity among both results is observed. The reflection coefficient response is analyzed from 4 GHz to 14 GHz. The effects are simulated with a step size of 0.1 GHz. There are six bands observed with the S_{11} value less than −10 dB. The first band was observed over the 4.611 to 4.921 GHz frequency with the S_{11} of −11.38 dB. The second band was observed over 5.071 to 5.561 GHz, with a reflection coefficient response of −24.08 dB. The third band represents a reflection coefficient response of −18.84 dB over the range from 7.531 to 7.881 GHz. The fourth band was observed over the 8.671 to 9.041 GHz, with the reflection coefficient response of −30.43 dB. The fifth band represents a reflection coefficient response of −14.72 dB over the 9.951 to 10.381 GHz. The last band was observed over the frequency span of 10.671 to 11.071 GHz, providing a reflection coefficient response of −49 dB. The peak value of the reflection coefficient response of −49 dB was observed in the sixth band.

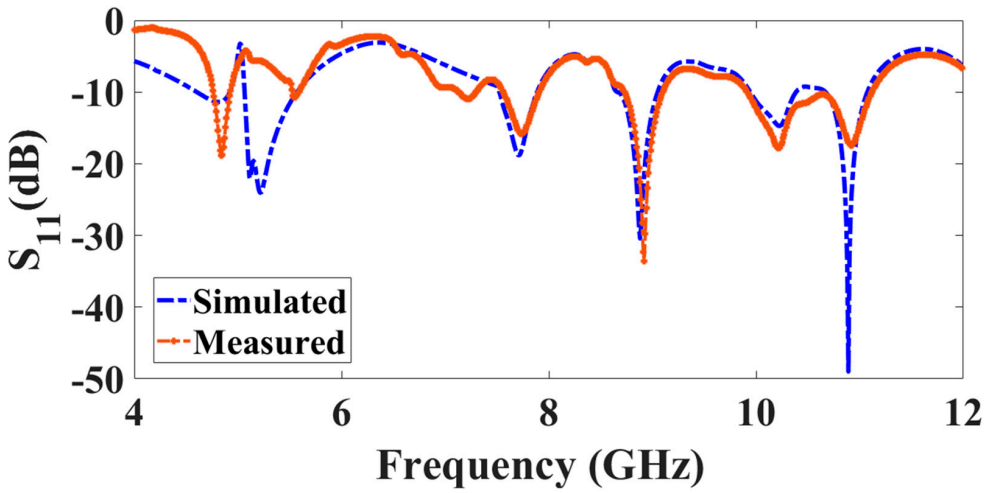

Figure 10. The simulated and measured multibands of reflection coefficient response over the frequency range from 4 GHz to 12 GHz. Overall, six band responses are observed in the proposed work.

The proposed design provides a narrow-band response for the different resonating frequencies. The narrow-band optical receiver operating for 5.2 GHz is suitable for radio-over-fiber communication applications [32]. The endless phase shifters (EPS) operating at 7.7 GHz are utilized in space diversity combining networks of digital microwave communication systems [33]. The application for aeronautical mobile communications operates at 8.8 GHz [34]. The resonance at 10.8 GHz is used in autonomous cars and communication systems for vehicle networking [35]. The performance of different structures in summary form is represented in Table 1. The four influential bands with a reflection coefficient response of less than −15 dB are considered. Their response is analyzed regarding directivity, gain response, electric field, and radiation pattern.

Antenna directivity represents the intended intensity concerning the average power in all directions [36]. The higher directivity value also represents the higher gain value [26]. The efficiency of the structure directly relates to the gain and directivity. The peak directivity of 0.6 dB is attained in the planned design, shown in Figure 11. The normalized directivity response is shown in Figure 12. The normalized directivity is measured over the zero to −3 dB range. The normalized directivity is observed in the −28 to 64 degrees (92 degrees) range. Further analysis of gain, electric field and the radiation pattern is considered for the less than −15 dB of the reflection coefficient response.

Table 1. The summary of all presented results.

Band	First	Second	Third	Fourth
Resonating Frequency (GHz)	5.22	7.771	8.881	10.891
Reflection coefficient Response (dB)	−24.08	−18.84	−30.43	−49.00
Range of Tuning (GHz)	5.071–5.561	7.531–7.881	8.671–9.041	10.671–11.071
Bandwidth (MHz)	490	350	370	400

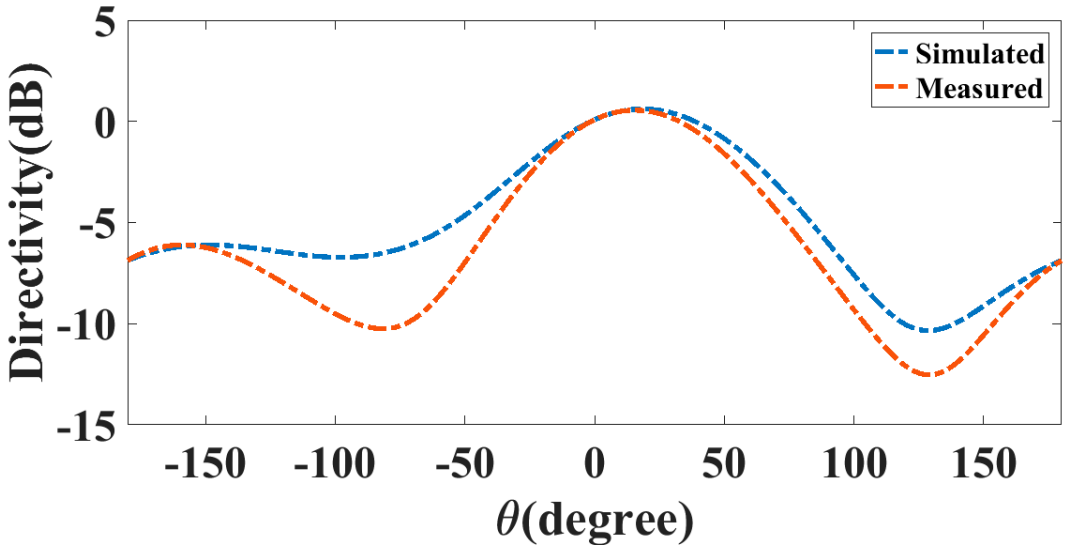

Figure 11. The measured and simulated directivity plot of the presented design.

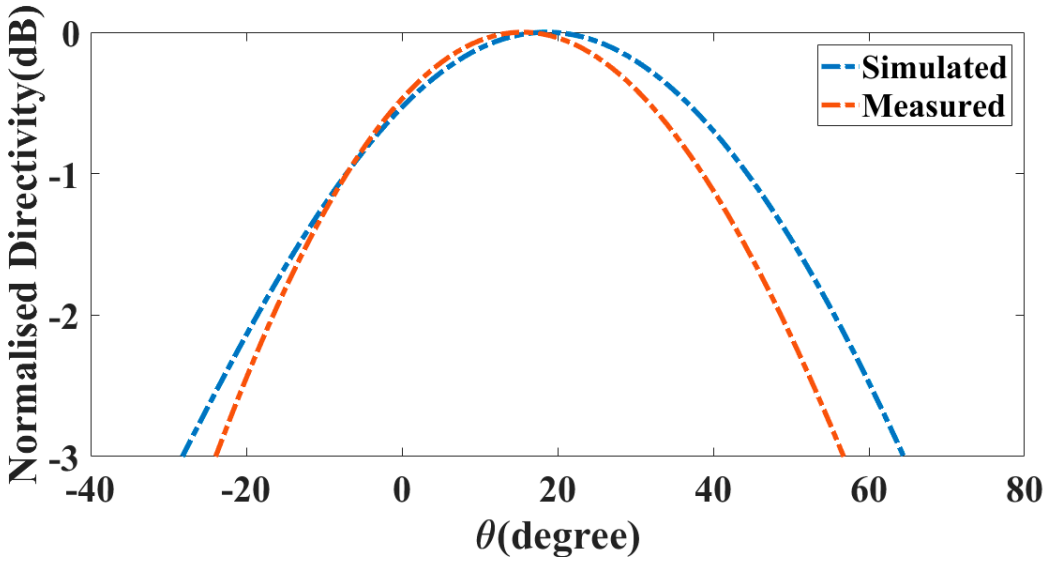

Figure 12. The presented design's normalized measured and simulated directivity plot.

The antenna gain represents the maximum radiation intensity concerning the average intensity in all directions [37]. The gain and directivity represent the efficiency of the proposed design structure. Therefore, achieving a positive gain for all resonating frequencies is necessary. Figure 13 represent the total gain of the proposed design structure for the different resonating frequency. The value of the total gain for the different frequencies 5.221 GHz, 7.771 GHz, 8.880 GHz and 10.891 GHz is, respectively, 0.53 dB, 2.39 dB, 2.61 dB and 5.77 dB.

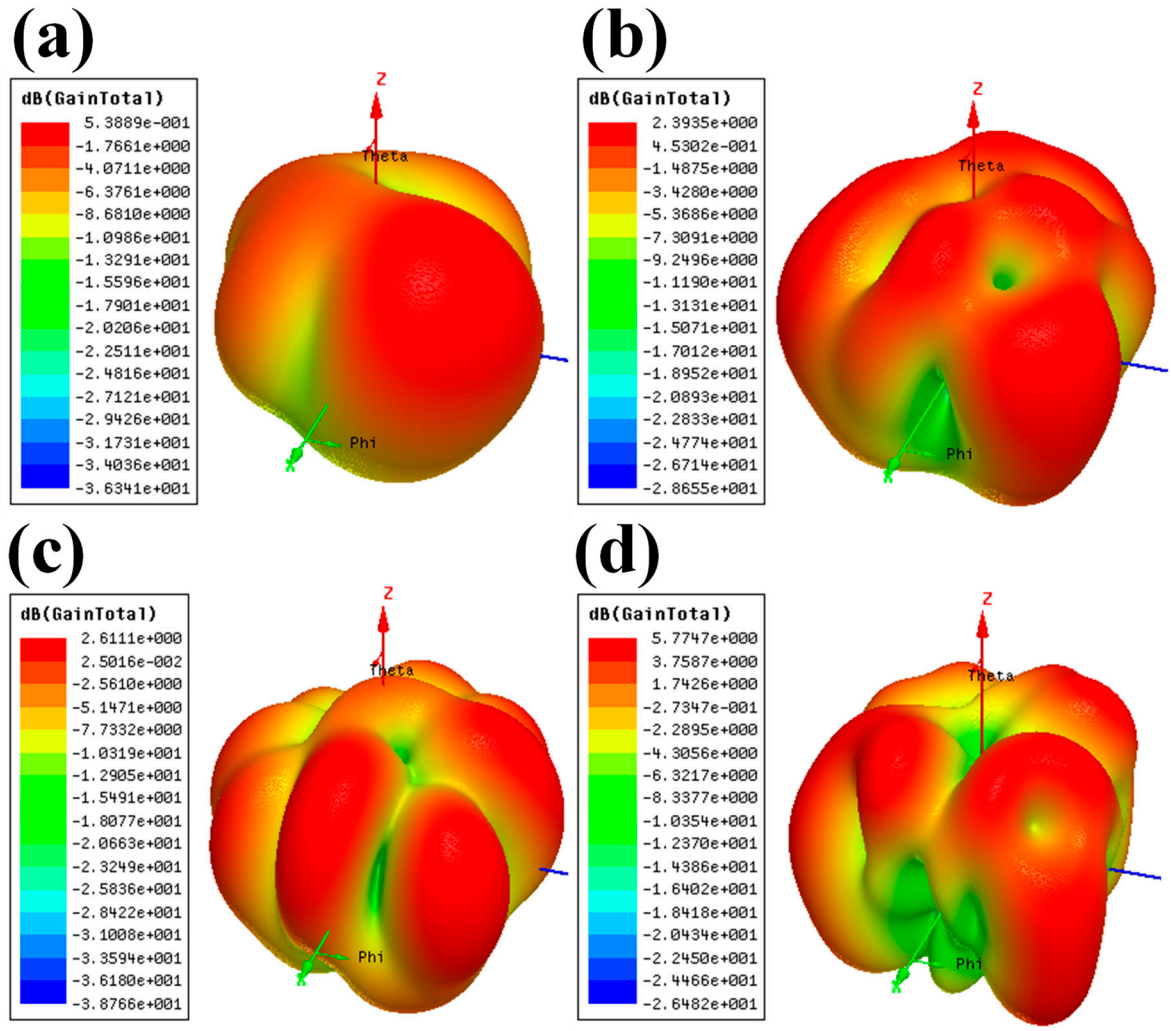

Figure 13. Total gain plot presented design. (**a**) The gain for resonating frequency of 5.221 GHz is 0.53 dB. (**b**) The gain for resonating frequency of 7.771 GHz is 2.39 dB. (**c**) The gain for resonating frequency of 8.880 GHz is 2.61 dB. (**d**) The gain for resonating frequency of 10.891 GHz is 5.77 dB. The notation used for gain plot: 5.3889e-001 = 0.53 × 10^{-1}. The same notation used for all figures.

The effective permeability $\left(\mu_{eff}\right)$, permittivity $\left(\varepsilon_{eff}\right)$ and impedance $\left(Z_{eff}\right)$ are measured using the scattering (S) parameters, and by taking the help of these parameters, the refractive index $\left(n_{eff}\right)$ can be calculated [38,39]. The ting discrepancy in the Q factor between the theoretical calculations and the numerical estimates provides direct proof for the crucial coupling that permits exceptional total absorption. Yet, when complete absorption through critical coupling can be achieved, the perfect absorber's impedance should equal that of the space (Z0 = 1) at the resonant wavelength from the perspective of the macroscopic electromagnetics. Therefore, Equation (6) is used to determine the effective impedance of a proposed structure [40].

$$\varepsilon_{eff} = \frac{n_{eff}}{Z_{eff}} \tag{4}$$

$$\mu_{eff} = n_{eff} \times Z_{eff} \tag{5}$$

$$Z_{eff} = \sqrt{\frac{(1+S_{11})^2 - S_{21}^2}{(1-S_{11})^2 - S_{21}^2}} \tag{6}$$

$$n_{eff} = \frac{1}{k_0 d}\left\{\mathrm{Im}\left[\ln\left(e^{ink_0d}\right)\right] + 2m\pi - i\mathrm{Re}\left[\ln\left(e^{ink_0d}\right)\right]\right\} \tag{7}$$

$$e^{ink_0d} = \frac{S_{21}}{1 - S_{11}\left(\frac{z-1}{z+1}\right)},\ k_0 = \frac{2\pi f}{c} \tag{8}$$

The speed of light is represented by c (m/s), and resonating frequency is f. The substrate thickness is d, and the branch index is m.

The metamaterial property of the structure helps to achieve miniaturization and improve the performance of a system. The different shapes of the metallic rings create the metamaterial property in the structure. The rings can be in the shape of circular, elliptical, triangular or rectangular shape. Metamaterial property is represented based on the impedance plot, shown in Figure 14. The resonating behavior of the real and imaginary values represents the impedance behavior of the presented design structure. The two-dimensional radiation pattern of the planned design structure is shown in Figure 15. The far-field measurement for the proposed design is carried out in the anechoic chamber. The normalized radiation pattern for the different resonating frequencies is considered. The analysis is carried out for the resonating frequencies of 5.22 GHz, 7.771 GHz, 8.881 GHz and 10.891 GHz. Overall broader directivity is observed for the different resonating frequencies. The behavior of any design structure is represented in a better way using the surface current distribution. The charge distribution varies according to the different resonating frequencies. Since the radiation intensity at each point in space matches the resultant radiation from the antenna's small parts, it leads to the result variations. The frequency-dependent radiation pattern is a sum of the vectorial, and the radiation intensity from the various elements has different path lengths in terms of wavelength. The path difference will affect the phase difference as the wavelength decreases, causing a rapid drop in the radiation intensity with a deviation angle from the peak radiation intensity. The number of side lobes may also change.

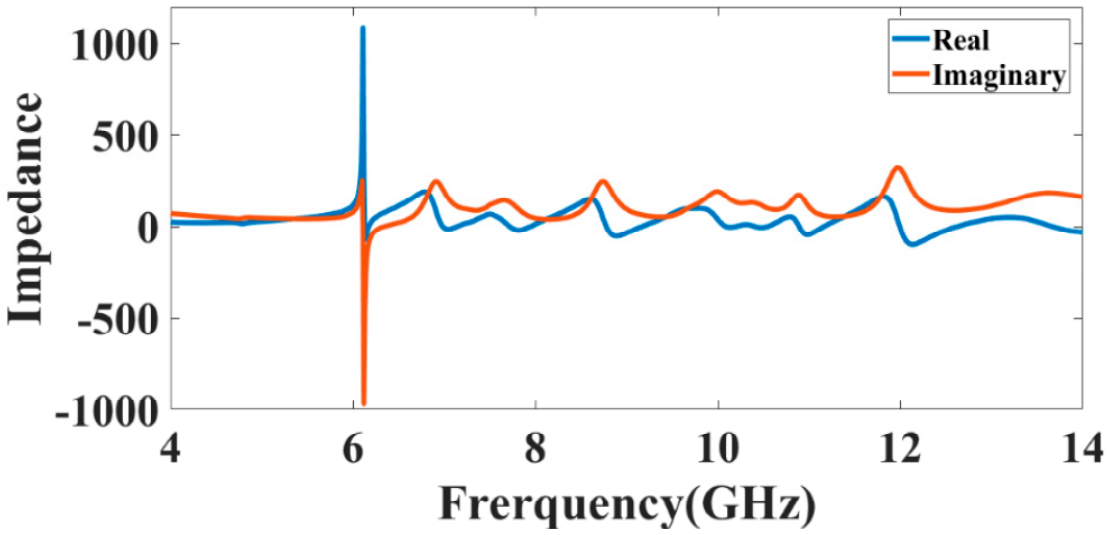

Figure 14. The metamaterial behavior representation of the proposed design structure using the impedance plot.

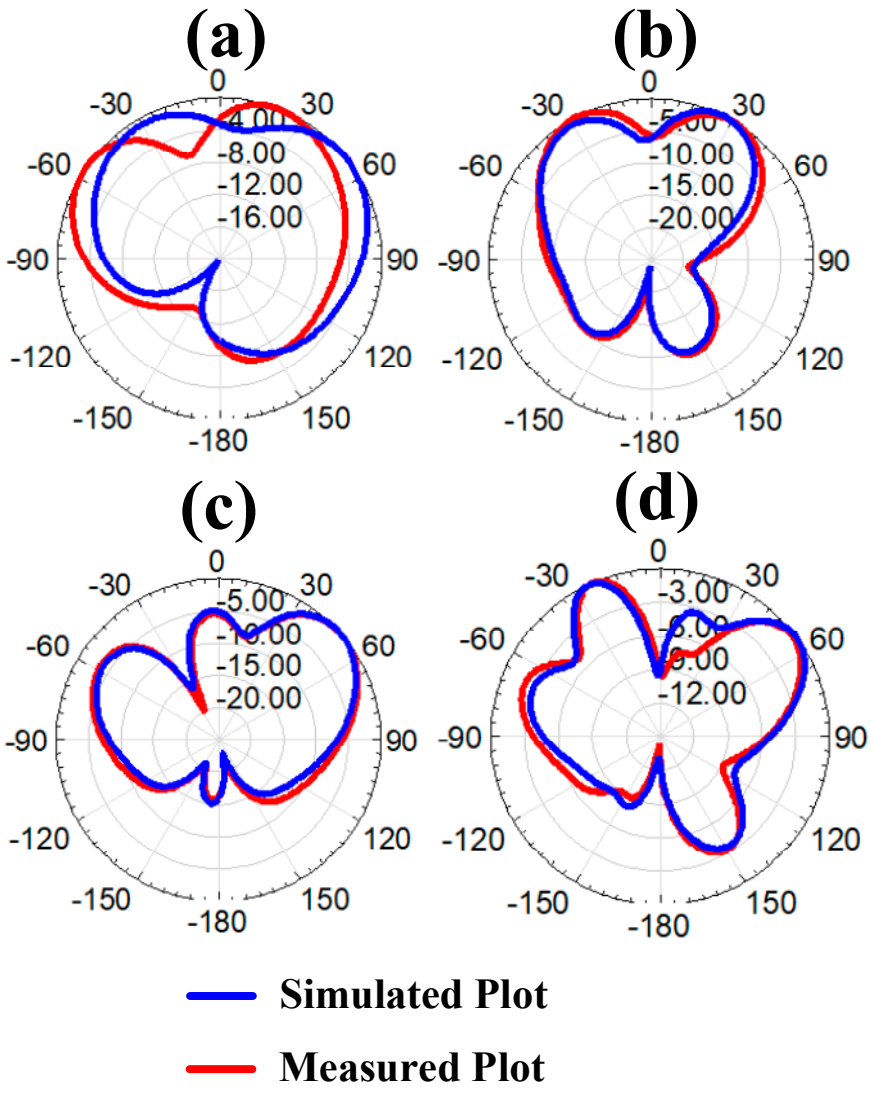

Figure 15. Two dimensional normalized measured and simulated radiation pattern (**a**) 5.22 GHz, (**b**) 7.771 GHz, (**c**) 8.881 GHz, (**d**) 10.891 GHz.

The aperture illumination also fluctuates due to the antenna's resonates at different frequencies. As the frequency varies, the current will flow in different directions, and peaks and nulls will be situated elsewhere. Moreover, according to the essential equation $G(\theta,\varphi) = (4\pi A(\theta,\varphi))/\lambda^2$, the wavelength varies with frequency. Consequently, altering the frequency will alter the antenna's emission pattern [41].

The values of the surface charge distribution of the proposed structure are represented in Figure 16. The surface charge distribution for the resonating frequency of 5.55 GHz is 1.29×10^4 V/m, 7.771 GHz is 8.94×10^3 V/m, 8.881 GHz is 8.15×10^3 V/m, 10.891 GHz is 8.15×10^3 V/m. The comparative study of the presented work with other articles is represented in Table 2. The comparison is given with five similar designs published before. The comparison shows that the proposed design performs better than the other designs in terms of bands, size, gain, etc. The size and number of bands are significant because they give the flexibility to be used simultaneously in different applications.

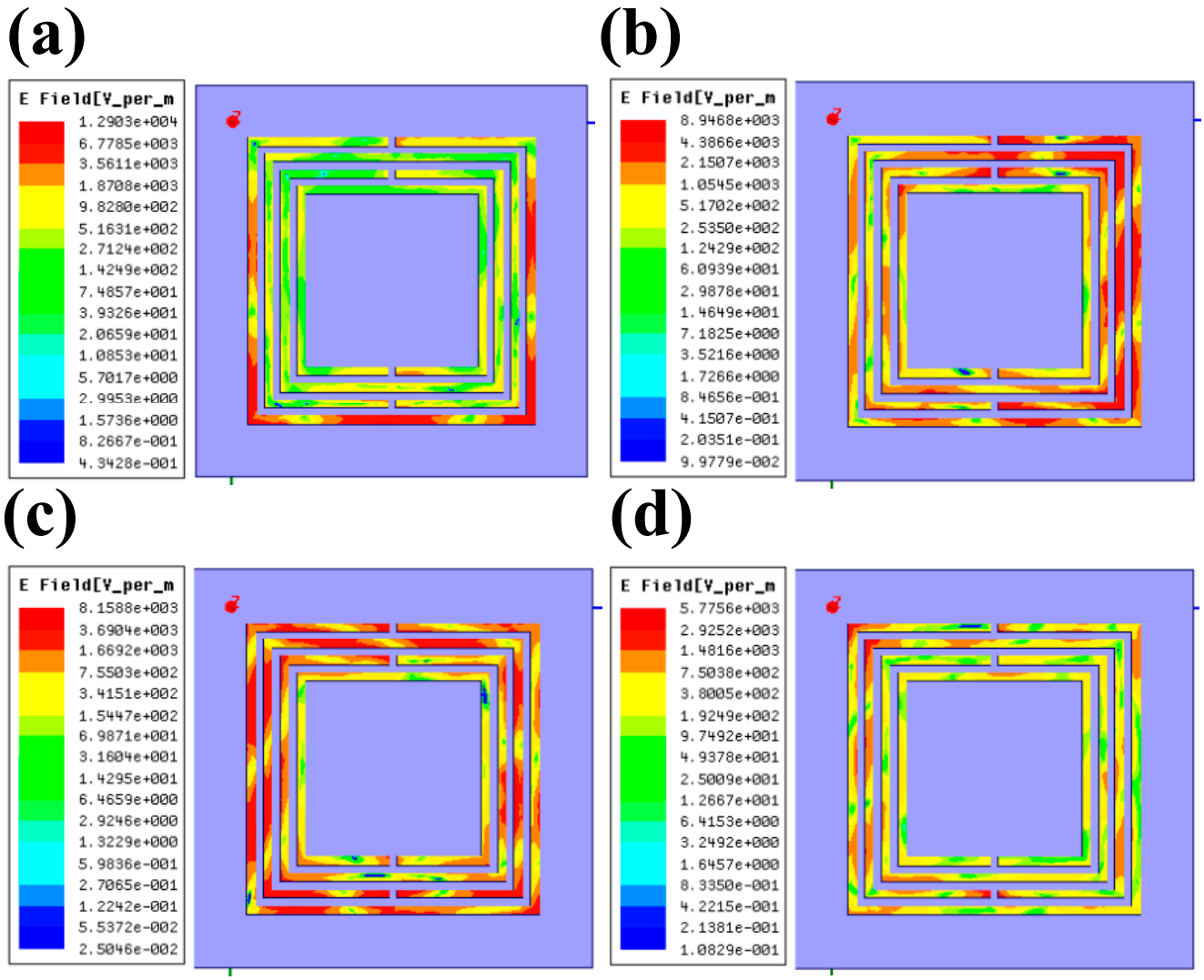

Figure 16. Surface charge distribution (**a**) 5.22 GHz, (**b**) 7.771 GHz, (**c**) 8.881 GHz, (**d**) 10.891 GHz. The notation used for electric field: 1.2903e+004 = 1.29 × 10^4. The same notation used for all figures.

Table 2. The comparative study of the presented design with other articles.

Reference	Total Bands	Size of Structure	Resonating Frequency (GHz)	Peak Gain
Proposed	6	48.2 × 48.2	4.8/5.22/7.771/8.881/10.2/10.891	5.77
[42]	2	45 × 40	2.4/5.5	2.34
[43]	3	40 × 50	1.65/1.93/2.20	2.93
[44]	2	75 × 140	0.698–0.960/1.710–2.690	-
[45]	3	22 × 25	2.4/3.5/5.8	3.15
[46]	5	24.8 × 30	2.28/2.65/4.80/5.89/8.73	3.01

5. Conclusions

The multiband, high gain and low-profile-based superstrate antenna are presented in this manuscript. The different approaches such as the varying height of superstrate layers, the feed position, the size of metamaterial rings, and the number of metamaterial rings, are considered and analyzed to identify the structure's optimized performance. Simulation and fabrication are analyzed by considering the low-profile FR4 material. Comparison among the measured and simulated responses of the reflection coefficient, radiation patten, and directivity is incorporated in the manuscript. The proposed design provides six

band response with sufficient bandwidth. The performance is analyzed regarding the reflection coefficient response, gain, directivity, E-field and radiation pattern. The FR4-based low-profile material is used in the presented work. The proposed design provides a maximum bandwidth of 490 MHz, a minimum reflection coefficient response of −49 dB, a peak gain of 5.77 dB, six bands response, proper directivity, an electric peak field of 1.29×10^4 V/m and a broader radiation pattern. Similarity among the simulated and measured results is observed. The low-profile material helps with the cost reduction in the proposed structure. The design highlights are compared with other published articles to identify the improvement. The multiband response over the 4 GHz to 12 GHz helps to attain multiple wireless communication applications such as WiFi and Microwave links.

Author Contributions: Conceptualization, A.A. and S.K.P.; methodology, A.A. and S.L.; software, S.L. and M.A.; validation, S.L., S.K.P. and M.G.D.; formal analysis, A.A. and S.L.; investigation, A.A. and K.A.; writing—original draft preparation, A.A., S.L., M.A., K.A., M.G.D. and S.K.P.; writing—review and editing, A.A. and S.K.P. All authors have read and agreed to the published version of the manuscript.

Funding: This research received no external funding.

Data Availability Statement: The data will be made available at a reasonable request to the corresponding author.

Conflicts of Interest: The authors declare no conflict of interest.

References

1. Yao, Y.; Chen, W.; Chen, X.; Yu, J. Analysis and Design of a Novel Multiband Antenna for Mobile Terminals. *Int. J. Antennas Propag.* **2015**, *2015*, 591269. [CrossRef]
2. Malallah, R.; Shaaban, R.M.; Al-Tumah, W.A.G. A Dual Band Star-Shaped Fractal Slot Antenna: Design and Measurement. *AEU–Int. J. Electron. Commun.* **2020**, *127*, 153473. [CrossRef]
3. Patel, S.K.; Lavadiya, S.P.; Parmar, J.; Ahmed, K.; Taya, S.A.; Das, S. Low-Cost, Multiband, High Gain and Reconfigurable Microstrip Radiating Structure Using PIN Diode for 5G/Wi-MAX/WLAN Applications. *Phys. B Condens. Matter* **2022**, *639*, 413972. [CrossRef]
4. Li, Y.; Yu, W. A Miniaturized Triple Band Monopole Antenna for WLAN and WiMAX Applications. *Int. J. Antennas Propag.* **2015**, *2015*, 146780. [CrossRef]
5. Li, Y.; Li, W.; Ye, Q. A Compact Asymmetric Coplanar Strip-Fed Dual-Band Antenna for 2.4/5.8 GHz Wlan Applications. *Microw. Opt. Technol. Lett.* **2013**, *55*, 2066–2070. [CrossRef]
6. Yao, Y.; Yu, J.; Chen, X. Compact Multi-Band Planar Antenna Design. In Proceedings of the 2012 Asia Pacific Microwave Conference Proceedings, Kaohsiung, Taiwan, 4–7 December 2012; pp. 1328–1330.
7. Yu, K.; Li, Y.; Wang, Y. Multi-Band Metamaterial-Based Microstrip Antenna for WLAN and WiMAX Applications. In Proceedings of the 2017 International Applied Computational Electromagnetics Society Symposium ACES 2017, Firenze, Italy, 26–30 March 2017; pp. 1–2.
8. Yoon, C.; Choi, S.H.; Lee, H.C.; Park, H.D. Small Microstrip Patch Antennas with Short-Pin Using a Dual-Band Operation. *Microw. Opt. Technol. Lett.* **2008**, *50*, 367–371. [CrossRef]
9. Kumar, A.; Pharwaha, A.P.S. On the Design of Novel Half T-Square Strip Fractal Antenna. *Int. J. Electron.* **2021**, *108*, 1774–1789. [CrossRef]
10. Dadhich, A.; Deegwal, J.K.; Sharma, M.M. Multiband Slotted Microstrip Patch Antenna for TD-LTE, ITU and X-Band Applications. In Proceedings of the 2018 5th International Conference on Signal Processing and Integrated Networks (SPIN), Noida, India, 22–23 February 2018; pp. 745–748.
11. Snehalatha, T.K.A.C.; Kumar, N. Design of Multiband Planar Antenna. In Proceedings of the 2017 IEEE International Conference on Antenna Innovations & Modern Technologies for Ground, Aircraft and Satellite Applications (iAIM), Bangalore, India, 24–26 November 2017; pp. 1–4.
12. Naik, S.; Chari, A. Design of a Multiband Microstrip Patch Antenna for 4G Application. In Proceedings of the 2020 IEEE International Conference for Innovation in Technology (INOCON), Bangluru, India, 6–8 November 2020; pp. 1–4.
13. Sran, S.S.; Sivia, J.S. ANN and IFS Based Wearable Hybrid Fractal Antenna with DGS for S, C and X Band Application. *AEU–Int. J. Electron. Commun.* **2020**, *127*, 153425. [CrossRef]
14. Weng, Z.-B.; Jiao, Y.-C.; Zhang, F.-S.; Song, Y.; Zhao, G. A Multi-Band Patch Antenna on Metamaterial Substrate. *J. Electromagn. Waves Appl.* **2008**, *22*, 445–452. [CrossRef]
15. Jaydeep, S.; Sunil, L. An Investigation on Recent Trends in Metamaterial Types and Its Applications. *i-manager's J. Mater. Sci.* **2018**, *5*, 55. [CrossRef]

16. Sharma, N.; Singh Bhatia, S. Split Ring Resonator Based Multiband Hybrid Fractal Antennas for Wireless Applications. *AEU–Int. J. Electron. Commun.* **2018**, *93*, 39–52. [CrossRef]
17. Sharma, N.; Bhatia, S.S. Metamaterial Inspired Fidget Spinner-Shaped Antenna Based on Parasitic Split Ring Resonator for Multi-Standard Wireless Applications. *J. Electromagn. Waves Appl.* **2020**, *34*, 1471–1490. [CrossRef]
18. Chaudhuri, S.; Kshetrimayum, R.S.; Sonkar, R.K. High Inter-Port Isolation Dual Circularly Polarized Slot Antenna with Split-Ring Resonator Based Novel Metasurface. *AEU–Int. J. Electron. Commun.* **2019**, *107*, 146–156. [CrossRef]
19. Samson Daniel, R.; Pandeeswari, R.; Raghavan, S. Multiband Monopole Antenna Loaded with Complementary Split Ring Resonator and C-Shaped Slots. *AEU–Int. J. Electron. Commun.* **2017**, *75*, 8–14. [CrossRef]
20. Kumar, A.; Althuwayb, A.A.; Chaturvedi, D.; Kumar, R.; Ahmadfard, F. Compact Planar Magneto-electric Dipole-like Circularly Polarized Antenna. *IET Commun.* **2022**, *16*, 2448–2453. [CrossRef]
21. Kumar, A.; Imaculate Rosaline, S. Hybrid Half-Mode S.I.W. Cavity-Backed Diplex Antenna for on-Body Transceiver Applications. *Appl. Phys. A* **2021**, *127*, 834. [CrossRef]
22. Kumar, A.; Chaturvedi, D.; Raghavan, S. Dual-Band, Dual-Fed Self-Diplexing Antenna. In Proceedings of the 13th European Conference on Antennas and Propagation, Krakow, Poland, 31 March–5 April 2019.
23. Rosaline, I.; Kumar, A.; Upadhyay, P.; Murshed, A.H. Four Element MIMO Antenna Systems with Decoupling Lines for High-Speed 5G Wireless Data Communication. *Int. J. Antennas Propag.* **2022**, *2022*, 9078929. [CrossRef]
24. Ameen, M.; Mishra, A.; Chaudhary, R.K. Asymmetric CPW-Fed Electrically Small Metamaterial- Inspired Wideband Antenna for 3.3/3.5/5.5 GHz WiMAX and 5.2/5.8 GHz WLAN Applications. *AEU–Int. J. Electron. Commun.* **2020**, *119*, 153177. [CrossRef]
25. Sharma, V.; Lakwar, N.; Kumar, N.; Garg, T. Multiband Low-cost Fractal Antenna Based on Parasitic Split Ring Resonators. *IET Microw. Antennas Propag.* **2018**, *12*, 913–919. [CrossRef]
26. Patel, S.K.; Lavadiya, S.P.; Parmar, J.; Ahmed, K.; Taya, S.A.; Das, S. Design and Fabrication of Reconfigurable, Broadband and High Gain Complementary Split-Ring Resonator Microstrip-Based Radiating Structure for 5G and WiMAX Applications. *Waves Random Complex Media* **2022**, 1–31. [CrossRef]
27. Rajak, N.; Chattoraj, N.; Mark, R. Metamaterial Cell Inspired High Gain Multiband Antenna for Wireless Applications. *AEU–Int. J. Electron. Commun.* **2019**, *109*, 23–30. [CrossRef]
28. Hansen, R.C. Fundamental Limitations in Antennas. *Proc. IEEE* **1981**, *69*, 170–182. [CrossRef]
29. Hertz, H. Ueber Strahlen Electrischer Kraft. *Ann. Der Phys.* **1889**, *272*, 769–783. [CrossRef]
30. Lavadiya, S.P.; Patel, S.K.; Ahmed, K.; Taya, S.A.; Das, S.; Babu, K.V. Design and Fabrication of Flexible and Frequency Reconfigurable Antenna Loaded with Copper, Distilled Water and Seawater Metamaterial Superstrate for IoT Applications. *Int. J. RF Microw. Comput. Eng.* **2022**, *32*, e23481. [CrossRef]
31. Patel, S.K.; Lavadiya, S.P.; Parmar, J.; Das, S.; Ahmed, K.; Taya, S.A. Low-Cost, Compact, and Reconfigurable Antennas Using Complementary Split-Ring Resonator Metasurface for next-Generation Communication Systems. *Int. J. Microw. Wirel. Technol.* **2022**, 1–11. [CrossRef]
32. Xiao, P.; Wang, Z. 5.2 GHz CMOS Narrow-Band Optical Receiver for Radio-Over-Fiber. In Proceedings of the 2006 International Conference on Communications, Circuits and Systems, Guilin, China, 25–28 June 2006; pp. 1937–1941.
33. Dhekial, R.P.; Bilagi, C.S. Endless Phase Shifter—Analysis and Design for 7.4 to 7.7 GHz Band. *IETE Tech. Rev.* **1993**, *10*, 247–256. [CrossRef]
34. Kaushal, D.; Shanmuganantham, T. Design of a Compact and Novel Microstrip Patch Antenna for Multiband Satellite Applications. *Mater. Today Proc.* **2018**, *5*, 21175–21182. [CrossRef]
35. Chung, M.-A.; Tseng, K.-C.; Meiy, I.-P. Antennas in the Internet of Vehicles: Application for X Band and Ku Band in Low-Earth-Orbiting Satellites. *Vehicles* **2023**, *5*, 55–74. [CrossRef]
36. Aliqab, K.; Lavadiya, S.; Alsharari, M.; Armghan, A.; Daher, M.G.; Patel, S.K. Design and Fabrication of a Low-Cost, Multiband and High Gain Square Tooth-Enabled Metamaterial Superstrate Microstrip Patch Antenna. *Micromachines* **2023**, *14*, 163. [CrossRef]
37. Sumathi, K.; Lavadiya, S.; Yin, P.Z.; Parmar, J.; Patel, S.K. High Gain Multiband and Frequency Reconfigurable Metamaterial Superstrate Microstrip Patch Antenna for C/X/Ku-Band Wireless Network Applications. *Wirel. Netw.* **2021**, *27*, 2131–2146. [CrossRef]
38. Smith, D.R.; Vier, D.C.; Koschny, T.; Soukoulis, C.M. Electromagnetic Parameter Retrieval from Inhomogeneous Metamaterials. *Phys. Rev. E* **2005**, *71*, 036617. [CrossRef] [PubMed]
39. Szabo, Z.; Park, G.-H.; Hedge, R.; Li, E.-P. A Unique Extraction of Metamaterial Parameters Based on Kramers–Kronig Relationship. *IEEE Trans. Microw. Theory Tech.* **2010**, *58*, 2646–2653. [CrossRef]
40. Li, H.; Qin, M.; Wang, L.; Zhai, X.; Ren, R.; Hu, J. Total Absorption of Light in Monolayer Transition-Metal Dichalcogenides by Critical Coupling. *Opt. Express* **2017**, *25*, 31612. [CrossRef] [PubMed]
41. Antar, Y.M.M. *Microstrip Antenna Design Handbook*; Artech House: Norwood, MA, USA, 2003; Volume 45, ISBN 0890065136.
42. Zhu, J.; Eleftheriades, G.V. Dual-Band Metamaterial-Inspired Small Monopole Antenna for WiFi Applications. *Electron. Lett.* **2009**, *45*, 1104. [CrossRef]
43. Sarkar, D.; Saurav, K.; Srivastava, K.V. Multi-band Microstrip-fed Slot Antenna Loaded with Split-ring Resonator. *Electron. Lett.* **2014**, *50*, 1498–1500. [CrossRef]
44. Chen, H.-D.; Yang, H.-W.; Sim, C.-Y.-D. Single Open-Slot Antenna for LTE/WWAN Smartphone Application. *IEEE Trans. Antennas Propag.* **2017**, *65*, 4278–4282. [CrossRef]

45. Ali, T.; Biradar, R.C. A Compact Multiband Antenna Using λ /4 Rectangular Stub Loaded with Metamaterial for IEEE 802.11N and IEEE 802.16E. *Microw. Opt. Technol. Lett.* **2017**, *59*, 1000–1006. [CrossRef]
46. Ali, T.; Mohammad Saadh, A.W.; Biradar, R.; Anguera, J.; Andújar, A. A Miniaturized Metamaterial Slot Antenna for Wireless Applications. *AEU–Int. J. Electron. Commun.* **2017**, *82*, 368–382. [CrossRef]